# Understanding Structure and Electronic Properties of $Th^{4+}$ - Water Complexes

Christophe Gourlaouen[1,2*], Carine Clavaguéra[3], Aude Marjolin[1,4],
Jean-Philip Piquemal[4*], Jean-Pierre Dognon[1*,]

1) CEA/Saclay, UMR 3299 CEA/CNRS SIS2M, Laboratoire de Chimie de coordination des éléments f, 91191 Gif-sur-Yvette, France,
2) Laboratoire de Chimie Quantique, ICS, UMR 7177, Université de Strasbourg, 4, rue Blaise Pascal, 67081 Strasbourg Cedex, France
3) Laboratoire des mécanismes réactionnels, Département de chimie, Ecole polytechnique, CNRS, 91128 Palaiseau cedex, France,
4) UPMC, Univ. Paris 6, UMR 7616, Laboratoire de Chimie Théorique, case courrier 137, 4 place Jussieu, F-75005 Paris, France,

E-mail contacts : gourlaouen@unistra.fr (C. G., Strasbourg);
jpp@lct.jussieu.fr (J.-P. P, UPMC);
jean-pierre.dognon@cea.fr (J.-P. D., CEA Saclay)

**Abstract**

In this contribution, we present a systematic quantum chemistry study of the $[Th(H_2O)_n]^{4+}$ (n=1 to 10) complexes to gain insight into their electronic structure and properties: the effect of the ligand distribution on the valence shells of the Thorium(IV) ion is studied by means of the Electron Localization Function (ELF) topological analysis. Particular care is given to the study of the monoaqua complex both at its equilibrium geometry, using various tools such as Energy Decomposition Analyses (EDA), and along its dissociation pathway. Indeed, as several electronic states cross the $Th^{4+}$-$H_2O^0$ ground state along the minimum energy path, we demonstrate that the diabatic representation implemented in MOLPRO is able to generate reference potential energy surfaces which will lead to the evaluation of diabatic dissociation curves. The calculated diabatic interaction energy curve will allow for a consistent parameterization of new generation force fields dedicated to heavy metals based on quantum chemistry.

**Keyword:** actinide, quantum chemistry, diabatic dissociation curve, Thorium, energy decomposition analysis, Electron Localization Function**.**

## Introduction

The f-block comprises the lanthanide series from La (Z=57) to Lu (Z=71) and the actinide series from Ac (Z=89) to Lr (Z=103). The use of the former elements has recently been widely spread in a variety of industrial fields, such as catalysis, medical diagnosis (contrast agents for medical resonance imaging) or organic light emitting diode displays[1]0[3][4], while the main application of the latter mostly resides in the field of nuclear energy[5][6][7], i.e. as fuel for nuclear power plants. As such, the chemistry of actinide cations and their compounds has to be investigated at the different stages of the nuclear cycle: from combustion to nuclear waste management. However, most of these cations are highly toxic either chemically or because of their radioactivity, and would therefore require devoted laboratories for their experimental study.

Consequently, computational chemistry can be of great help by allowing the in silico probing of the properties of actinide compounds and their environment, as well as the modeling of their response and behavior. However, new difficulties arise for the theoretical study of f-elements as compared namely to transition metals. For instance, the high nuclear charge of the elements implies to take into account relativistic effects[8]; also, the presence of open shells in both neutral and ionic forms of the metal, due to partially occupied d and f shells, requires the use of accurate but expensive theoretical methods. Such approaches are possible for small systems but not for the chemically relevant ones, which generally include the cation, polydentate cryptants and an aqueous solvent.

Therefore, for these large systems, only long-time scale classical molecular dynamics (MD) simulations can be used though recent studies on lanthanide and actinide compounds have shown that one could not perform significant MD simulations on heavy elements compounds without a polarizable force field[9][10][11][12][13][14]. Indeed, in a high-dielectric medium such as water and/or with strongly charged ions, polarization affects the geometry of complexes as well as intermolecular interactions. Polarizable force fields try to account for these many-body effects including an explicit term in the potential energy function to treat polarization of charge distributions by the environment[15] [16].

As a polarizable force field with an optimized water model, the AMOEBA potential has proved to be particularly well suited to the modeling of lanthanide elements[9][10]. Furthermore, being entirely parameterized on ab initio data, no experimental information is required, which,

in the case of lanthanide and actinide systems are rare or unavailable. The required ab initio data for the building of such a potential is the dissociation curve between the ion and a reference molecule, which was chosen to be water. Additional information includes the electric dipole polarizability of the ion. Previous studies investigating the influence of relativistic effects on the static electric dipole polarizability of $La^{3+}$ to $Lu^{3+}$ ions and $An^{4+}$ ions[18][19] have shown that accurate results are only obtained including scalar relativistic effects, core polarization and flexibility of the basis sets.

The use of high level, though mono-reference methods, to compute the dissociation curves, of closed-shell or high-spin lanthanide ions, such as $Gd^{3+}$, has proved to be a reasonable approach. However, in the event of charge transfer between the ion – generally actinyl[20] or actinide cations - and the ligand, multi configurational approaches need to be considered. Indeed, the charge transfer phenomena was observed by Hagberg et al[21] between the high spin open shell Cm(III) ion and a water molecule along the dissociation pathway of the dimer, indicating that the system ionized to $Cm^{2+}$ and $H_2O^+$. A means of reducing the charge transfer phenomenon used by the authors was to introduce a second water molecule, which is kept fixed during the dissociation. The interaction energy curve was computed at CASSCF/CASPT2 level with an active space consisting of the outermost 7s, 6d and 5f orbitals of the cation, but neglecting any orbitals from the ligand. More recently, electron transfer was also observed between the highly charge closed shell Th(IV) and a water molecule by Réal et al.[14]. The carried out MRCI+DC calculations, with an active space including the empty 6d and 5f orbitals of Thorium as well as the highest occupied molecular orbital of the ligand, i.e. the nonbonding O($\pi$) orbital, showed that this charge transfer lead to $Th^{3+}$-$H_2O^+$ and $Th^{2+}$-$H_2O^{2+}$ complexes at the dissociation limit. However, due to convergence failure of the MRCI+DC calculations, the active space was redefined in such a way that charge transfer to the 6d orbitals of Th(IV) was forbidden. Consequently, no energy point was obtained at distances within the critical region of the charge transfer.

In this contribution, we present the dissociation of the $[Th(H_2O)]^{4+}$ complex with accurate quantum chemistry methods, complete with a diabatization procedure which allows for the computation of the diabatized MRCI interaction energy curve for subsequent force field building. Relativistic effects are also investigated in this model system. Furthermore, a detailed study of the different $[Th(H_2O)_n]^{4+}$ complexes (n = 1 to 10) is presented based on several theoretical chemistry tools to give an overview of their electronic and structural properties. Energy Decomposition Analyses quantifies the electrostatic character of the Th-O bond due to the high positive charge of the ion while the Electron Localization Function

topological analysis is used to better understand the electronic structures of the complexes.

**Computational details**

In a first step, four-component (4c) all-electron calculations using a full Dirac-Coulomb Hamiltonian at the Hartree-Fock level (DHF) were carried out using the DIRAC08[22] program to provide reference data for the $[Th(H_2O)]^{4+}$ system. The geometry of the complex was fully optimized at three different levels of approximation: 4c Levy-Leblond[23] (non relativistic, NR), 4c-spin-free Dirac-Coulomb[24] (scalar relativistic effects only, SF-DHF) and 4c Dirac-Coulomb (including scalar relativistic effects and spin-orbit coupling, DHF). Dyall's uncontracted triple zeta basis set [33s29p20d13f5g2h] was used for Thorium[25] and Dunning's uncontracted aug-cc-pVTZ basis set for the oxygen and hydrogen atoms[26], DIRAC software and used basis set are thereafter referred as SET 1. The kinetic balance requirement is fulfilled by deriving the small-component basis set from the basis functions of the large components. The reliability of the basis set was checked on the energy of the $Th^{4+}$ ion with respect to numerical Multi-Configuration Dirac-Fock calculations obtained with the MCDFGME v2005.10 program package[27]. However, the simultaneous treatment of the relativistic effects and the electronic correlation in the fully relativistic four-component framework is very computational demanding and cannot be used to derive a full dissociation curve. Keeping that in mind, the one-component framework was tested using Dolg et al. quasi-relativistic effective core potential (ECP) for Thorium and associated ANO basis set[28]. The calculations were performed with the MOLPRO 2008.1[29] program package at RHF, MP2, CCSD(T), MCSCF, MRCI and DFT levels. MOLPRO software and basis set used are thereafter referred as SET 2. The CI binding energy are given with Davidson correction when specified. [30]

The whole Thorium aqua series was studied using the GAUSSIAN09[31] package. Calculations were performed at the HF, MP2 (all electrons correlated) and DFT levels using the small core pseudo potential and associated basis set[32] for Th and Pople's 6-31+G(d,p) basis for Oxygen and Hydrogen[33] (Software and basis thereafter referred as SET 3). The basis set superposition error (BSSE) was estimated by the counterpoise procedure[34]. Natural Population Analyses were performed on the optimized structures. The discussed Thorium complexes are all minima, checked by a frequency calculation, except when specified. The ELF analysis was performed at HF level from the GAUSSIAN data using the DGRID[35] package.

The Thorium-water binding energies ΔE are computed in two different ways. For single-reference wave functions, this energy is expressed as the difference of the energy of the complex and the energy of its fragments (equation 1).

$$(1)\ \Delta E = E(Th^{4+}\text{-}H_2O) - E(Th^{4+}) - E(H_2O)$$

For multi-reference calculations such a definition is no longer valid. In those cases, binding energies are estimated by the difference of the energy at a given Th-O distance and that at the Th-O distance of 50 Å. Zero Point Energies (ZPE) and Gibbs free energies (ΔG) are estimated from standard statistical thermodynamics (ideal gas assumed) after calculation of the harmonic vibrational frequencies.

Energy Decomposition Analyses were performed using the GAMESS US[36] software with a CRENBL[37] large core pseudo potential (78 core electrons) (defining SET 4) following the Reduced Variational Space (RVS) procedure[38] at the Hartree-Fock level. In the RVS scheme, the total binding energy (ΔE) between the cation and the water molecules is decomposed in several physical terms. The first two terms result from the frozen Molecular Orbitals of the isolated fragments and represent the electrostatic interaction ($E_{elec}$) and the exchange-repulsion ($E_{exrep}$) contributions. Then, as the orbitals of the two fragments are progressively relaxed, the polarization energy ($E_p$), i.e. the distortion of the orbital of a fragment in the field generated by the "frozen" fragment is computed; followed by the charge transfer energy ($E_{ct}$), i.e. the contribution of electron transfer from occupied orbitals of one fragment to the vacant orbitals of the other fragment. The last term (δE) accounts for some higher-order many-body terms from different physical origins that are not detailed in the standard RVS decomposition; they are expected to be negligible with respect to ΔE as in the RVS scheme the antisymmetry of the wavefunction is maintained (see reference [39] for details). Note that since we performed such computations at the HF level, no dispersion contribution could be included

## Results and discussion

### I. Study of $[Th(H_2O)]^{4+}$

#### 1) General considerations

To understand the relative importance of relativistic effects with respect to electronic correlation effects both on interaction energies and geometries, a step-by-step comparison is proposed from non-relativistic calculations to a full 4-component framework. Full geometry optimizations were performed on the $[Th(H_2O)]^{4+}$ system in the $C_{2v}$ symmetry at various levels, and **Table 1** presents the resulting geometries and bonding energies. When comparing DHF and nonrelativistic results, relativity provides small modifications of the water molecule geometry but brings a significant decrease in the bonding energy. Also, the Th-O distance is lengthened. This behavior was already observed by Mochizuki et al.[40] for the $f^0$ monoaqua complexes of the $La^{3+}$ and $Ac^{3+}$ ions. One possible explanation is the relativistic destabilization of the accepting d and f spinors of Thorium which weakens the Th-O bond. Accordingly, the decrease in the bonding energy, about 7 % including relativity (DHF vs. NR), is in line with the calculated elongation of the metal-oxygen distance. The Mulliken charge of Thorium does not vary significantly at the HF level with or without relativistic effects. It can also be observed that, upon taking into account relativistic effects, the charge transfer towards the 5f and 6d orbitals of Thorium decreases due to a loss of the accepting character of these orbitals. As such, our results are in agreement with those of Mochizuki and Tsushima[41] of a Th-O bond length of 2.23 Å and bonding energy of 152.0 $kcal.mol^{-1}$ at DHF level, and 2.21 Å and 166.3 $kcal.mol^{-1}$ at MP2 level, though with a smaller basis set. The comparison of DHF and SF-DHF results shows that the spin-orbit coupling has no effect both on the bonding energy and on the geometry, with respect to the scalar relativistic calculations. In a one-component Hartree-Fock framework, the results obtained with the quasi-relativistic effective core potential are in very good agreement with the four-component ones. Consequently, this one-component approach can be used to further explore the electronic correlation effects while decoupled from spin-orbit coupling effects. Computed MP2 and CCSD(T) results for the $[Th(H_2O)]^{4+}$ system are very similar: at both levels of theory, the Th-O distance is shortened and the bonding energy is increased as compared with HF/DHF results. DFT yields very similar geometries while still overestimating the bonding energy, especially with the PBE functional. Calculations of the isolated cation show that this is related to the important stabilization of the 5f and 6d orbital. The HOMO-LUMO gap in $Th^{4+}$ is

reduced from 1.27 Hartree at RHF level to 0.70 Hartree with DFT/PBE (SET 3). This makes these empty orbital much more accepting and explain, the greater binding energies.

**2) Population, EDA and topological analyses**

As expected for such a charged complex, the binding energy is mostly ensured by electrostatic interactions between ligand and metal, as well as the polarization of the ligand (see **Table 2**). No back-donation is observed, with a charge transfer contribution from $Th^{4+}$ to $H_2O$ ($E_{ctth}$) close to zero and a negligible cation polarization energy. These statements are highlighted by the Natural Population Analyses (NPA) presented in Table 3 for the monoaqua complex of Thorium. It can also be pointed out that the 5f orbitals contribute significantly and are active in this complex at B3LYP level and, to a lesser extent, at HF level.

Specific structures appear in the ELF analysis performed on the HF wave function. In **Figure 1**, the value of the ELF function is plotted in the $\sigma_v$ plane of the molecule containing the four atoms. The central core basin of Thorium is not affected by the coordination of a water molecule. However, the external "subvalence" (see reference [42] for a detailed discussion about the notion of metals "subvalence basin") of Thorium is strongly distorted compared to that of the isolated cation, resulting in the splitting into two separate basins. One is located at opposite the water molecule and the other one is an annulus closer to the ligand. These basins roughly correspond to the sum of the full 6s and 6p electrons and the donation to the empty 6d and 5f orbitals, as shown by the electron population of the ELF basin (around 8.2 electrons) and the radius of the basin (around 1 Å) that can be compared to the radius of maximum radial density of the 6s (0.76 Å), 6p (0.82 Å and 0.92 Å) and 6d orbitals (1.27 Å and 1.32 Å) (see data in reference [43]). This perturbation of the external shell of the cation is easily explained by comparing the basins of the isolated fragments and those of the complex. **Figure 2** reports the evolution of the ELF function upon complexation along the $C_2$ axis of the complex and the difference in electronic density between the complex and the fragments. The curves show the extension of the ELF basins of the cation and the water molecule at the Th-O equilibrium distance. Without perturbation, there is a superposition of the ELF basins corresponding to the water lone pair and to the Thorium external shells. Electronic repulsion leads to a deformation of these basins appearing along the molecular $C_2$ symmetry axis. In line with the water polarization observed within EDA, a displacement of the oxygen electronic density towards the Thorium ion occurs. This is characterized by a decrease of the electronic density near the oxygen core and an increase at intermediate distance. The $Th^{4+}$

cation itself is also affected since, despite a formal small polarizability, the external core shell of the cation splits into two distinct basins (**Figure 1**) due to the presence of the water molecule. There is also a decrease of the electronic density close to the Thorium ion in the direction of the ligand with an increase in the opposite direction. The water molecule indeed modifies the electronic distribution of the $Th^{4+}$ cation.

### 3) Th-O dissociation

**Preliminary considerations.** With the aim being the building of a molecular mechanics potential from ab initio reference results, the interaction energy curve of the $[Th(H_2O)]^{4+}$ complex has to be computed. It has already been shown that upon dissociation, potential energy surface crossings occur between the $An^{x+}$ - $H_2O$ state and $An^{(x-1)+}$ - $H_2O^+$ (x=3,4) states for such highly charged cations as observed for $Cm^{3+}$ and $Th^{4+}$[12][14]. In both cases, the authors circumvent the surface crossing through extra approximation[14] (i.e. not considering the involved 6d orbitals of Thorium) or by adding a second water molecule[12]. In this paragraph, we show that this problem can also be solved using a diabatization procedure as implemented in MOLPRO[44].

Partial geometry optimizations were performed using the $C_{2v}$ symmetry at various levels of theory using single- or multi-reference wave functions and both GGA and hybrid DFT functionals. The Th-O distance was optimized, whereas the O-H distance and H-O-H angle in water were kept frozen in the gas phase experimental geometry[45] (i.e. 0.957 Å and 104.5°). Freezing of the geometry of the water molecule is required as the diabatization procedure can only be applied to one dimension of the potential energy surface. The evolution of the Th-O distance and bonding energy results at water frozen geometry are similar to the completely relaxed geometry one (see **Table 1** and **Table 4**) whatever the level of theory. Adding the constraints leads to an increase of the Th-O bond length of about 0.025 Å and a 5 $kcal.mol^{-1}$ drop of the bonding energy. The effect of the methods on these characteristics is similar for both systems.

Also, whatever the level of theory, the BSSE is small and does not exceed 0.7 kcal/mol, i.e. 0.5% of the total interaction energy. It will therefore be neglected in further calculations. For multi-reference calculations, several active spaces were considered in order to find the best compromise between accuracy and computational resources usage (i.e. the smallest significant active space). Calculations were done in $C_{2v}$ group to take advantage of symmetry in such highly resource demanding calculations. The 2p lone pair of oxygen of $b_1$ symmetry

being the highest occupied orbital of the complex, the active space was consequently restricted to orbitals of the $b_1$ subgroup, since and due to symmetry conservation of the wave function, no single electron transfer is possible from other subgroup orbitals ($a_1$, $b_2$ or $a_2$). The active space is then built upon the full 2p oxygen orbital, two 5f and one 6d empty orbitals of Thorium exhibiting the proper symmetry and MRCI computations were performed using this active space. In other word, the diabatization was performed using CASSCF[2,4] wavefunction. The MRCI level is thus taken as reference: the bonding energy between $Th^{4+}$ and one water molecule is -160.4 kcal.mol$^{-1}$ with an equilibrium Th-O distance of 2.217 Å. The comparable values with CCSD(T) indicates that the main part of the electronic correlation is provided by the dynamic correlation and at the equilibrium geometry, the complex is mainly single-reference (90% weight). The other contributions are provided by some charge transfer between the water lone pair and the $Th^{4+}$ orbitals (5f, 6d).

**Adiabatic dissociation curve.** The $[Th(H_2O)]^{4+}$ adiabatic dissociation curves computed using an MCSCF wave function are given in **Figure 3**. With the CASSCF[2,4] wavefunction, ten configurations are generated. At the equilibrium distance (2.217 Å) the ground state ($S_0$) corresponds to the neutral water. Then three states ($S_1$-$S_3$) are energetically close and above $S_0$. These states correspond to the single ionization of the water molecule with an electron transfer towards the empty 5f and 6d orbitals of the thorium cation. All the higher states ($S_4$-$S_9$) correspond to the double ionization of the water molecule.

At about 2.6 Å, the $S_0$ surface crosses a higher lying $S_1$ surface. The crossing results in a net charge transfer that leads to $Th^{3+}$-$H_2O^+$. The third state ($S_2$) is very close to the first ones (about 10 kcal.mol$^{-1}$) and could be involved in an avoided crossing, while the fourth state ($S_3$) is well separated. A large number of very close lying-states ($S_4$ to $S_9$) can also be seen in **Figure 3**. Several crossings with the $S_3$ state occur in the dissociation path beyond 6.0 Å. The process results in a double ionization of the water molecule. It should be noted that due to the relatively limited active space, the higher states might not be realistic. The analysis of the wave function shows that the charge transfer occurs from the 2p(O) to the 5f(Th) orbitals for the first crossing, while the third state $S_2$ is consistent with a charge transfer from the 2p(O) to the 6d(Th) orbitals. To obtain accurate energies, MRCI calculations were performed from a set of MCSCF configurations. The adiabatic MRCI wave function includes single and double excitations out of the active space.

All MRCI results are shown in **Figure 4** and should be analyzed as follows. First, the crossings are shifted to larger distance, e.g., at about 3.0 Å for the first one. Then, the

dynamic correlation strongly stabilizes the closed shell singlet state with respect to the excited states. The analysis of the MRCI wave function at the equilibrium geometry shows that the ground state is not purely closed shell with a significant contribution of about 15% from single excitations terms. After the crossing, these contributions vanish leading to a now closed shell state. The two next states are a mix of two configurations corresponding to one electron in the 5f and one electron in the 6d orbitals of Thorium, the respective weights being 56/44 % for $S_1$ and 44/56 % for $S_2$. After the surface crossing, the states become quasi-degenerated, and are transformed into pure configurations ($5f^1$ configuration for $S_1$ and $6d^1$ configuration for $S_2$). At both MCSCF and MRCI levels, the $5f^1$ configuration is stabilized by about 23 $kcal.mol^{-1}$ with respect to the $6d^1$ one. The charge transfer from $Th^{4+}$-$H_2O$ occurs essentially from the 2p(O) water orbitals to the 5f(Th) orbitals leading to $Th^{3+}$-$H_2O^+$.

Due to the surface crossing, the dissociation cannot provide a correct path, i.e., $[Th(H_2O)]^{4+} \rightarrow Th^{4+} + H_2O$, that is required to extract parameters for force field developments. For that purpose, it is necessary to apply diabatization methods.

**Diabatic dissociation curve.** In this section, we discuss the general topology of the diabatic MRCI dissociation curves for the $[Th(H_2O)]^{4+}$ model system. In these calculations, the quasi-diabatization procedure proposed by Simah, Hartke, and Werner was used to obtain diabatic dissociation curves between the ground and excited states[44]. The quasi-diabatic wavefunctions (and the corresponding CI vectors) are established so that they vary as little as possible as a function of the geometry. The diabatization is carried out by maximizing the overlap for all the pairs of active orbitals at the reference geometry with those at neighborhood geometry using a Jacobi rotation technique. Preferably, the adiabatic and diabatic states should be identical at the reference geometry, e.g., due to symmetry. Indeed, it is necessary to monitor the modification of the nature of the states after the surface crossing, making the choice of the reference geometry a major difficulty. For instance, taking the reference at the equilibrium distance gives a correct behavior before the surface crossing but not after. On the contrary, taking the reference after the crossing produces an erroneous behavior before the crossing. In order to find a solution to this problem, we propose to modify the reference wave function at the equilibrium geometry in the following procedure. If, in a standard calculation, all the states have the same weight in the reference, here, the modified reference is built from the equilibrium geometry (Th-O distance equal to 2.217 Å) by increasing the ground state weight with respect to the excited states. The reference curve is chosen in order to satisfy the rule above, i.e., the adiabatic and diabatic states should be

identical at the reference geometry. **Figure 5** shows the different results when varying the ground state weight for the reference state (30, 60 and 90%). The best fit with the adiabatic $S_0$ curve at the reference geometry is obtained for the $E_3$ curve. Of course, to choose the best compromise, the correct asymptotic behavior towards the $Th^{4+}+H_2O$ dissociation limit of the adiabatic $S_3$ curve must be achieved. This is not the case for the $E_0$ curve while the $E_1$ and $E_2$ curves match exactly the reference adiabatic $S_3$ asymptote at 4.2 Å, though beyond, only the $E_3$ curve keeps a right behavior. The difference is due to an artificially strengthened weight of the charge transfer states in the ground state wave function at the reference point, as a consequence of the state average procedure. The more the charge transfer weight in the ground state wave function, the more the deviation between the adiabatic and diabatic curves. The $E_3$ curve is the only one which satisfies all the criteria defined previously both at the equilibrium geometry and at the dissociation limit. It can therefore be used to extract parameters for force field developments. For this diabatized MRCI interaction energy curve, the resulting bonding energy is -159.6 $kcal.mol^{-1}$ at the Th-O equilibrium distance of 2.217 Å. Of course, the choice of larger active spaces is always possible and debatable. Here, the definition of the active space was made in such a way as to propose the best compromise between the inclusion of physically meaningful orbitals and the computational cost limitations induced by the diabatization procedure. Thanks to increase of computer power, there is no doubt that we should be able to improve our results a step further in the coming years. In any case, the proposed strategy will remain valid providing a non-empirical way to obtain a diabatic dissociation curve that could be applied to a wide range of problem including the determination of force field parameters[46].

To conclude, despite the simplicity of the system, i.e. only four atoms and a closed-shell singlet state, the electronic structure appears more complex than expected. There are discrepancies between DFT and wave function methods, since both functionals used in this study lead to an overestimation of the Th-O binding energy. This is associated to a larger charge transfer in DFT than in wave function theory (WFT)[50] occurring mainly through the 6d orbital of Thorium with some contribution of 7s and 5f orbitals. However, EDA shows that even if charge transfer is non-negligible, the preponderant terms are the polarization energy of the water molecule and the charge-charge interaction. Also ELF shows that the subvalence basins of the Thorium cation appear perturbed by the presence of the water molecule. Upon coordination the basin splits following the electronic rearrangement around the Thorium ion when coordinated to the ligand. Finally, the $[Th(H_2O)]^{4+}$ dissociation curve has been computed using a diabatization procedure to avoid charge transfer induced state crossings and

retain the $Th^{4+}$ - $H_2O$ ground state configuration. The resulting diabatic dissociation curve has been used to extract polarizable force field parameters for the study of the $Th^{4+}$ ion hydration.[46]

## II. Study of $[Th(H_2O)_n]^{4+}$

### 1) Geometric considerations

The following section deals with the higher order aqua complexes of the Thorium ion, up to the more meaningful and physical octa-, nona- and deca-coordinated system. First, concerning the diaqua complex, only few computations have been performed[40][41]. Mochizuki and Tsushima proposed 4-component relativistic calculations on an assumed $D_{2h}$ symmetry of the system. Starting with the same structure, we found it to be a third-order saddle point and therefore considered four other possible geometries of the diaqua complex. The MP2 optimized geometries are reported in **Figure 6** and shows that the O-Th-O angle is weakly sensitive to the computational level (see **Table 5**) in the 110-117° range. The least stable structures are the ones referred to as $D_{2h}$ and $C_{2v}(2)$ and exhibit imaginary frequencies. The energy difference between the $C_{2v}(1)$ and $C_2$ complexes is quasi nil, though the first one is a transition state in all cases except at B3LYP level, the imaginary frequency corresponding to the out-of-plane mode of the hydrogen atoms. In the $C_2$ symmetry, the two water molecules are not exactly in the O-Th-O plane but deviate by about 15° from planarity. The rotation of the water molecules in order towards orthogonality to the O-Th-O plane (see $C_{2v}(2)$ structure), destabilizes the complex by about 1 $kcal.mol^{-1}$, leading to a second order saddle point. The $D_{2h}$ structure lies higher in energy than the previous geometries by about 3 to 7 $kcal.mol^{-1}$. The addition of a second water molecule leads to a slight increase of the Th-O bond distance by 0.05 Å for all considered methods. All geometrical parameters are close within the $C_2$, $C_{2v}(1)$ and $C_{2v}(2)$ structures. The O-Th-O angle opens moving from $C_2$ to $C_{2v}(1)$ because of a larger interaction between the two facing hydrogen atoms. The opposite trend is observed when moving from $C_2$ to $C_{2v}(2)$ structures as the direct hydrogen interaction vanishes. The $D_{2h}$ symmetry leads to a slight increase of the Th-O bond, which will be explained in the following.

The geometries of the most stable conformation of the complexes from 3 to 10 water molecules are provided in Figure 7. The triaqua complex has a $C_3$ symmetry with O-Th-O angles around 105° and Th-O distances of 2.3 Å (see Table 6). The higher $D_3$ symmetry

structure is a transition state between two $C_3$ structures, located only 1.0 kcal.mol$^{-1}$ above the $C_3$ minimum at MP2 level. The tetraaqua complex is the first one with a homogeneous ligand distribution. It possesses a regular $S_4$ symmetry with Th-O bonds of 2.35 Å and Th-O angles of 109.5°, the oxygen atoms forming a tetrahedron around the cation. The pentaaqua complex is also a $C_{2v}$ structure: the distribution of the water molecules close to a triangular bipyramid though the two trans water molecules are far from linearity, the O-Th-O angle being around 145°. The symmetry of the hexaaqua complex is $T_h$, with an octahedral geometric arrangement of the oxygen atoms. The hepta and octa-coordinated systems have a $C_2$ and $S_8$ symmetry, respectively. As for the last complex, the oxygen atoms form a squared antiprism around the $Th^{4+}$. The nona-coordinated system is not truly the usual tricapped trigonal prism with $D_{3h}$ symmetry, but a $D_3$-symmetry structure due to the arrangement of the hydrogen atoms. A $C_s$ minimum was found for the tenfold coordinated system. All these structures correspond to minima on the potential energy surface. These structures exhibit lower symmetries than those found by Tsushima *et al.* who did not consider the hydrogen atoms. The groups found in this work are subgroups of Tsushima's symmetry groups. This is in line with the largest binding energies found in our work. However, the agreement on bond length is good and our results are consistent with this pioneer works. [47-49] For almost all complexes, all the Th-O distances are similar within a considered complex though this is no longer the case for n = 10 which possesses a short Th-O bond 2.587 Å and two long ones 2.660 Å (MP2). Upon coordination, there is a general increase of the Th-O bond length moving from 2.210 Å for n=1 to 2.610 Å (MP2) for n=10. In the same way, the O-Th-O angles of neighboring water molecules get smaller. All correlated methods lead to a slight contraction the Th-O bonds in comparison with HF results, typically by a range of 0.02 to 0.04 Å. This effect is more pronounced for MP2 which generally gives slightly more compact structures than PBE, itself leading to more compact structures than B3LYP.

### 2) Energetics

The total complexation energies (ZPE and BSSE corrected) and complexation free energies for $[Th(H_2O)_n]^{4+}$ (n=1 to 10) are reported in Table 7. Obviously, the complex stability increases upon successive coordination of water molecules. The coordination of a tenth water molecule is also favored, even when taking BSSE and ZPE corrections into account or considering free energies. Also, the relative energies of several Th(IV)-water aggregates with 8 to 10 water molecules were previously investigated at the MP2 level[14]. A coordination of

10 water molecules around the cation was also found to be stable, even if an "8+2" coordination-type is more favorable. Such energetic comparisons both at quantum chemistry level and using a polarizable force field are presented in our recent related paper[46].

In all cases, the correlated values are greater than the HF energies. The PBE functional leads to the largest complexation energies. For the non-BSSE corrected energies, there is a crossing between B3LYP and MP2 values for the heptacoordinated complex. MP2 attributes a greater stability of high coordinated complexes than B3LYP. The order of BSSE corrected energies is conserved for all the coordination numbers: PBE > B3LYP > MP2 > RHF. The ZPE correction is almost the same for all methods, roughly 2.4 kcal.mol$^{-1}$ per water molecule. Also, the BSSE is of the same order of magnitude (close to 2 kcal.mol$^{-1}$) except at MP2 level (around 4 kcal.mol$^{-1}$ per water molecule). This correction represents only 1% of the complexation energy for the monoaqua and 5% for the decaaqua complexes, except for MP2 for which it represents 10%.

### 3) Property analyses

**Population Analysis.** The charge transfer from the ligands to the Thorium ion calculated at HF, MP2 and B3LYP levels is reported in **Table 3**. Despite the bond length elongation, the charge transfer per water molecule remains almost constant. As in the mono aqua complex, it occurs mainly through the 6d orbitals of Thorium with some very small contributions of the 5f and 7s orbitals. No significant difference in the population analyses can be noted when considering the various structures. As expected, static correlation (MP2) weakly modifies the charge transfer and DFT increases it[50]. However, there is a discrepancy in the charge transfer nature between DFT and WFT. After a peak for hepta coordinated systems, the role of the 5f diminishes for WFT whereas it continues to increase for DFT. This is in line with the greater electroaffinity of 5f orbitals found in DFT as compared to WFT. Starting from the nine-coordinated complexes, the 7p orbitals of Thorium contribute also to donation because the expansion of the structures favors their overlap with the oxygen lone pairs.

**Topology.** The ELF analysis points out the existence of non-spherical Th(IV) basins around the cation (**Figure 8**). Such basins which are related to the outer-shell densities of the Th(IV) cation are formally core ones and are denoted as “subvalence basins”. Such a topological picture allows a discussion about the bonding capabilities of a metal cation. In line with its

small polarizability[19], the $Th^{4+}$ cation is commonly considered as a hard cation in the Pearson HSAB theory, but it exhibits a part of "soft character" as defined by the ELF approach[42]. This character corresponds to the fragmentation of the initially spherical outer ELF basin into several ones which reflects the non-spherical ligand distribution. Such effects have been shown to play a role in $Pb^{2+}$ complexes, for example[51]. In the present case, the ELF basins, corresponding to the full 6s, 6p and empty 6d and 5f orbitals, are distorted upon ligand coordination.

For the diaqua complex, two subvalence basins are located trans to each water molecules, which are quite diffuse (V = 21.7 $Å^3$, pop = 2.82 electrons). In addition, two smaller basins are located above and below the O-Th-O plane (V = 5.2 $Å^3$, pop = 1.59 electrons). This basin repartition is due to the non-linearity of the molecule. The relative position of the hydrogen atoms is not obvious, as the energy differences are around 1 $kcal.mol^{-1}$ between $C_2$ and $C_{2v}(2)$ structures. Despite these small values, the convergence of the results suggests that the out of plane distortion of the hydrogen distribution is not an artifact. We suppose that this orientation is due to a water-water interaction between the waters bond to the cation, probably the repulsion between the positively charged hydrogens hold by these ligand.

ELF analyses of low-coordinated geometries (n=2 or 3) show that the complexes tend to adopt less symmetric structures due to the $Th^{4+}$ external basin distortion (see ref. [42] for a detailed discussion on this phenomenon). For higher coordination numbers (n = 5 and 6), the steric congestion around the cation prevents the apparition of lacunary structures. However, similar structures are present. The external core basins of Thorium are split into several basins following the symmetry of the molecule. Figure 8 shows that there is an ELF minimum pointing towards each face of the polyhedron defined by the water molecules. For n=5, five basins are present with a major one located on the $C_2$ axis of the molecule, at the opposite of the water. For n=6, eight equivalent basins are located on $C_3$ axis of the regular octahedron formed by the waters. As for n=2, this external basin accounts for the 6s and 6p electrons along with the charge transferred on the 5f, 6d and 7s orbitals. However, a strong compression of this basin occurs, its volume decreasing rapidly from 49.3 (n=1) to 16.0 $Å^3$ (n=6). From the sixth fold complex, the compression of the external core basin stopped and its volume remain almost constant up to n=10, with a value of 14.4 $Å^3$. The core basin of Thorium is spherical in all cases.

## Conclusion

In this contribution, we investigated the structural and energetic features of the successive coordination of water molecules to the $Th^{4+}$ cation. For all coordination numbers ($1 \leq n \leq 10$), the lowest-energy minima exhibit lower symmetry than for the geometries obtained if only oxygen atoms are considered, due to the distribution of hydrogen atoms. Furthermore, for low coordination numbers, lacunar structures are observed through ELF analyses and are due to a deformation of the external core basin of Thorium in the presence of the water molecules. This property for $Th^{4+}$ is very similar to that of main-block element cations [51-52]. Ligand polarization and donation towards cation play an important role in the binding of water molecules on $Th^{4+}$ as highlighted by the EDA. The donation is ensured by the accepting 6d and 5f orbitals of Thorium according to NPA analysis with some contribution of the 7s and 7p orbitals for the largest sizes (n=9,10). Donation is the smallest for $[Th(H_2O)]^{4+}$ and the electron cloud of the water molecule is strongly polarized towards $Th^{4+}$ allowing for easy charge transfer towards the cation. Consequently, several avoided surface crossings occur upon Th-O dissociation, leading to curves unsuitable to build molecular mechanics force fields. However, the use of a diabatization procedure allowed us to recover the dissociation curve of the unique $Th^{4+}$ - $H_2O$ state. Correlation effects are quite important in describing the interactions, adding a 10% extra-stabilization to the formation of the complexes. DFT leads to more compact structures than WFT methods in line with a higher stabilization of the accepting 6d and 5f orbitals of Thorium. These contracted orbitals tend to shorten the Th-O distances to favor overlap with the donating water lone pairs and counterbalance the ligand-ligand repulsion. This is not the case in WFT since the 6d and 5f orbitals are not stable enough to compensate the Pauli repulsion. Despite these differences, the trends are similar for all methods, coordination of an extra water molecule is favored up to n = 10, even when taking into account BSSE, ZPE and entropic effects. The present ab initio work contributed to the building of a polarizable force field for the $Th^{4+}$ cation. From the quantum chemical interaction energies of the $Th^{4+}$-$H_2O$ dimer, a direct derivation of the van der Waals force field parameters was performed[46]. Again, concerning the presented ab initio methods, the choice of larger active spaces is always possible. Nevertheless, our strategy should remain valid as computer power increases, providing a non-empirical way to obtain diabatic dissociation curve that could be applied to a wide range of problems, including force field development along with the capability of performing energy decomposition analysis on both open-shell and closed-shell heavy metal complexes [53]. The proposed procedure already led

to simulation results on Th(IV) solvation that have been shown to be in excellent agreement with experimental results on structural, dynamical and thermodynamical properties[46]. Future works will focus on a systematic study of the solvation of lanthanide and actinide cations complexed to organic ligands.

**Acknowledgment**

We would like to thank Prof. H.J. Werner for fruitful discussions. We express our gratitude to Dr. Olivier Parisel for a careful reading of the manuscript. Two of the authors, C. G. and J.-P. D., thank the direction of simulation and experimental tools of the CEA nuclear energy division CEA/DEN/DSOE for financial support. This work was granted access to the HPC resources of [CCRT/CINES/IDRIS] under the allocation c2012086146 made by GENCI (Grand Equipement National de Calcul Intensif).

**References**

[1] Merbach, A. E.; Toth, E. *The Chemistry of Contrast Agents in Medical Magnetic Resonance Imaging*, Wiley, Chichester, **2001**.

[2] Bottrill, M.; Kwok, L.; Long, N. J. *Chem Soc Rev* **2006**, *35*, 557-571.

[3] Moore, E. G.; Samuel, A. P. S.; Raymond, K. N. *Acc Chem Res* **2009**, *42*, 542-552.

[4] Hou, Z.; Wakatsuki, Y. *Coord Chem Rev* **2002**, *231*, 1-22.

[5] Silva, R.; Nitsche, H. *Radiochim Acta* **1995**, *70*, 377.

[6] Grenthe, I.; Fuger, J.; Konings, R.; Lemire, R.; Muller, A.; Nguyen-Trung, C. Wanner, H. in *Chemical Thermodynamics of Uranium* (Eds.: Wanner, H.; Forest, I.), North-Holland, Amsterdam, **1992**.

[7] Nash, K. L.; Madic, C.; Mathur, J. N. in *The Chemistry of the Actinide and Transactinide Elements* (Eds.: Morss, L. R.; Edelstein, N. M.; Fuger; J.), Springer: Dordrecht, **2006**.

[8] Pyykko, P. *Chem Rev* **1988**, *88*, 563-594.

[9] Clavaguera, C.; Calvo, F.; Dognon, J.P. *J Chem Phys* **2006**, *124*, 074505.

[10] Clavaguera, C.; Sansot, E.; Calvo, F.; Dognon, J. P. *J Phys Chem B* **2006**, *110*, 12848-12851.

[11] Duvail, M. Martelli, F. ;Vitorge, P.; Spezia, R. *J Chem Phys* **2011**, *135*, 044503.

[12] Hagberg, D.; Karlström, G.; Roos, B. O.; Gagliardi, L. *J Am Chem Soc* **2005**, *127*, 14250-14256.

[13] Galbis, E.; Hernández-Cobos, J.; den Auwer, C.; Le Naour, C.; Guillaumont, D.; Simoni, E.; Pappalardo, R. R.; Sánchez Marcos, E. *Angew Chem Int Ed* **2010**, *49*, 3811-3815.

[14] Real, F.; Trumm, M.; Vallet, V.; Schimmelpfennig, B.; Masella, M.; Flament, J. P. *J Phys Chem B* **2010**, *114*, 15913-15924.

[15] Gordon, M. S.; Freitag, M. A.; Bandyopadhyay, P.; Jensen, J. H.; Kairys, V.; Stevens, W. J. *J Phys Chem A* **2001**, *105*, 293-307.

[16] Gresh, N.; Cisneros, G. A.; Darden, T. A.; Piquemal, J.-P. *J. Chem. Theory. Comput.* **2007**, 3, 1960-1986.

[17] Ponder, J. W.; Wu, C. J. ; Ren, P. Y.; Pande, V. S.; Chodera, J. D.; Schnieders, M.; Haque, I.; Mobley, D. L. ; Lambrecht, D. S.; DiStasio, R. A.; Head-Gordon, M.; Clark, G. N. I.; Johnson, M. E.; Head-Gordon, T. *J Phys Chem B* **2010**, *114*, 2549-2564.

[18] Clavaguera, C.; Dognon, J.P.; Pyykko, P. *Chem Phys Lett* **2006**, *429*, 8-12.

[19] Real, F.; Vallet, V.; Clavaguera, C; Dognon, J.P. *Phys Rev A* **2008**, *78*, 052502.

[20] Clavaguera-Sarrio, C.; Brenner, V.; Hoyau, S.; Marsden, C. J.; Millie, P.; Dognon, J. P. *J Phys Chem B* **2003**, *107*, 3051-3060.

[21] Hagberg, D. ; Bednarz, E.; Edelstein, N. M.; Gagliardi, L. *J Am Chem Soc* **2007**, *129*, 14136-14137.

[22] DIRAC, a relativistic ab initio electronic structure program, Release DIRAC08 (2008), written by Visscher, L.; Jensen, H. J. Aa.; Saue, T et al. (see http://dirac.chem.sdu.dk).

[23] Lévy-Leblond, J.-M. *Communications in Mathematical Physics* **1967**, *6*, 286-311.

[24] Dyall, K. G. *J Chem Phys* **1994**, *100*, 2118-2127.

[25] Dyall, K. G.*Theor Chem Acc* **2007**, *117*, 491-500.

[26] Dunning, T. H. *J Chem Phys* **1989**, *90*, 1007-1023.

[27] Desclaux, J.-P.; Indelicato, P. MCDFGME, MultiConfiguration Dirac Fock and General Matrix Elements program, release 2005, see http://dirac.spectro.jussieu.fr/mcd.

[28] Cao, X. Y. ; Dolg, M. ; Stoll, H. *J Chem Phys* **2003**, *118*, 487-496.

[29] MOLPRO is a package of ab initio programs written by Werner, H.-J., Knowles P. J., Lindh, R.; Manby, F. R.; Schütz, M., and others, MOLPRO, version 2008.1, a package of ab initio programs, 2008, see http://www.molpro.net.

[30] Davidson, E. R.; Silver, D. W. *Chem. Phys. Lett.* **1977**, *53*, 403-406

[31] Gaussian 09, Revision B.01, Frisch, M. J.; Trucks, G. W.; Schlegel, H. B.; Scuseria, G. E. and others, Gaussian, Inc., Wallingford CT, 2009.

[32] Kuchle, W.; Dolg, M.; Stoll, H.; Preuss, H. *J Chem Phys* **1994**, *100*, 7535-7542.

[33] Harihara, P. C.; Pople, J. A. *Theor Chim Acta* **1973**, *28*, 213-222.

[34] Boys, S. F.; Bernardi, F. *Mol Phys* **1970**, *19*, 553-566.

[35] Kohout M. DGrid, version 4.6, Radebeul, 2011

[36] Schmidt, M. W; Baldridge, K. K.; Boatz, J. A.; Elbert, S. T.; Gordon, M. S.; Jensen, J. H.; Koseki, S.; Matsunaga, N.; Nguyen, K. A.; Su, S.; Windus, T. L.; Dupuis, M.: Montgomery, J. A. *J. Comput. Chem.* **1993**, *14*, 1347-1363.

[37] Ermler, W. C.; Ross, R. B.; Christiansen, P.A. *Int J Quantum Chem* **1991**, *40*, 829-846.

[38] Stevens, W. J.; Fink, W. H. *Chem Phys Lett* **1987**, *139*, 15-22.

[39] Cisneros, G. A.; Darden, T. A.; Gresh, N.; Reinhardt, P.; Parisel, O.; Pilmé J. ;Piquemal J.-P. in Multi-scale Quantum Models for Biocatalysis: Modern Techniques and Applications, for the Book Series: Challenges and Advances in Computational Chemistry and Physics , ed. D. M. York and T.-S. Lee **2009**, 137-172, Springer Verlag

[40] Mochizuki, Y.; Tatewaki, H. *Chem Phys* **2001**, *273*, 135-148.

[41] Mochizuki, Y.; Tsushima, S. *Chem Phys Lett* **2003**, *372*, 114-120.

[42] de Courcy, B.; Pedersen, L. G.; Parisel, O.; Gresh, N.; Silvi, B.; Pilmé, J.; Piquemal, J.-P. *J Chem Theory Comput* **2010**, *6*, 1048-1063.

[43] Desclaux, J.P. *Atomic data and nuclear data tables* **1973**, *12*, 311-406.

[44] Simah, D.; Hartke, B.; Werner, H. J. *J Chem Phys* **1999**, *111*, 4523-4534.

[45] Benedict, W. S.; Gailar, N.; Plyler, E. K. *J Chem Phys* **1956**, *24*, 1139-1165.

[46] Marjolin, A.; Gourlaouen, C.; Clavaguera, C.; Ren, P. Y.; Wu, J.-C.; Gresh, N.; Dognon, J. P.; Piquemal, J.-P. *Theor Chem Acc* **2012**, *131*.

[47] Yang, T.; Tsushima, S.; Suzuki, A. *J. Phys. Chem. A* **2001**, *105*, 10439-10445

[48] Yang, T.; Tsushima, S.; Suzuki, A. *Chem. Phys. Lett.* **2002**, *360*, 534-542

[49] Tsushima, S.; Yang, T.; Suzuki, A.; Mochizuki, Y.; Okamoto, Y. *Chem. Phys. Lett.* **2003**, *375*, 204-212

[50] Piquemal, J.-P., Marquez, A.; Parisel, O.; Giessner-Prettre, C. *J Comput Chem* **2005**, *26*, 1052-1062.

[51] Gourlaouen, C.; Piquemal, J.-P.; Parisel, O. *J. Chem. Phys.,* **2006**, 124, 17, 174311.

[52] van Severen, M.-C.; Gourlaouen, C.; Parisel O. , *J Comput Chem* **2010**, *31*, 185-194.

[53] Marjolin, A.; Gourlaouen, C.; Clavaguera, C.; Dognon, J.-P.; Piquemal, J.-P. *Chem. Phys. Lett.*, **2013**, 563, 25

**Figures**

**Figure 1:** Cut-plane ELF representation for the isolated $Th^{4+}$ (left) and $[Th(H_2O)]^{4+}$ in the $\sigma_v$ plane (right). The red color corresponds to a local electron maximum. Calculation done with SET 2.

**Figure 2:** Values of the ELF function along the $C_2$ axis of the complex and of the fragments (top). Difference in electronic density between the complex and the fragments (bottom). Calculation Done with SET 2.

**Figure 3:** MCSCF adiabatic dissociation curve for $[Th(H_2O)]^{4+}$. Results obtained with SET 2.

**Figure 4:** MRCI adiabatic dissociation curve for $[Th(H_2O)]^{4+}$ from a set of MCSCF configurations. Results obtained with SET 2.

**Figure 5:** MRCI diabatic dissociation curve for $[Th(H_2O)]^{4+}$ using equilibrium geometry as reference and varying the weight of the different states. Results obtained with SET 2.

**Figure 6:** Structures of the $[Th(H_2O)_2]^{4+}$ complex and relative energies ($kcal.mol^{-1}$) (see Table 5) at MP2 level. Results obtained with SET 2.

**Figure 7**: Structures of the most stable conformation of the $[Th(H_2O)_n]^{4+}$ complexes (n = 3 to 10). Results obtained with SET 3.

**Figure 8:** 3D ELF representation (left, $\eta$ = 0.77) and cutplane representation (right) of the $[Th(H_2O)_2]^{4+}$ complex in $C_2$ symmetry ($1^{st}$ row), the $[Th(H_2O)_5]^{4+}$ ($2^{nd}$ row) and $[Th(H_2O)_6]^{4+}$ ($3^{rd}$ row) complexes. Results obtained with SET 3.

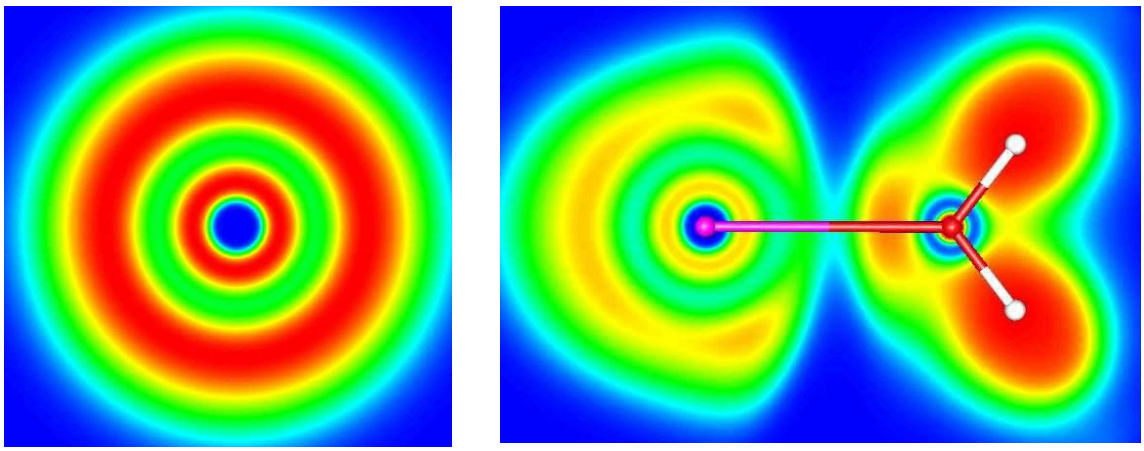

**Figure 1:** Cut-plane ELF representation for the isolated $Th^{4+}$ (left) and $[Th(H_2O)]^{4+}$ in the $\square_v$ plane (right). The red color corresponds to a local electron maximum. Calculation done with SET 2.

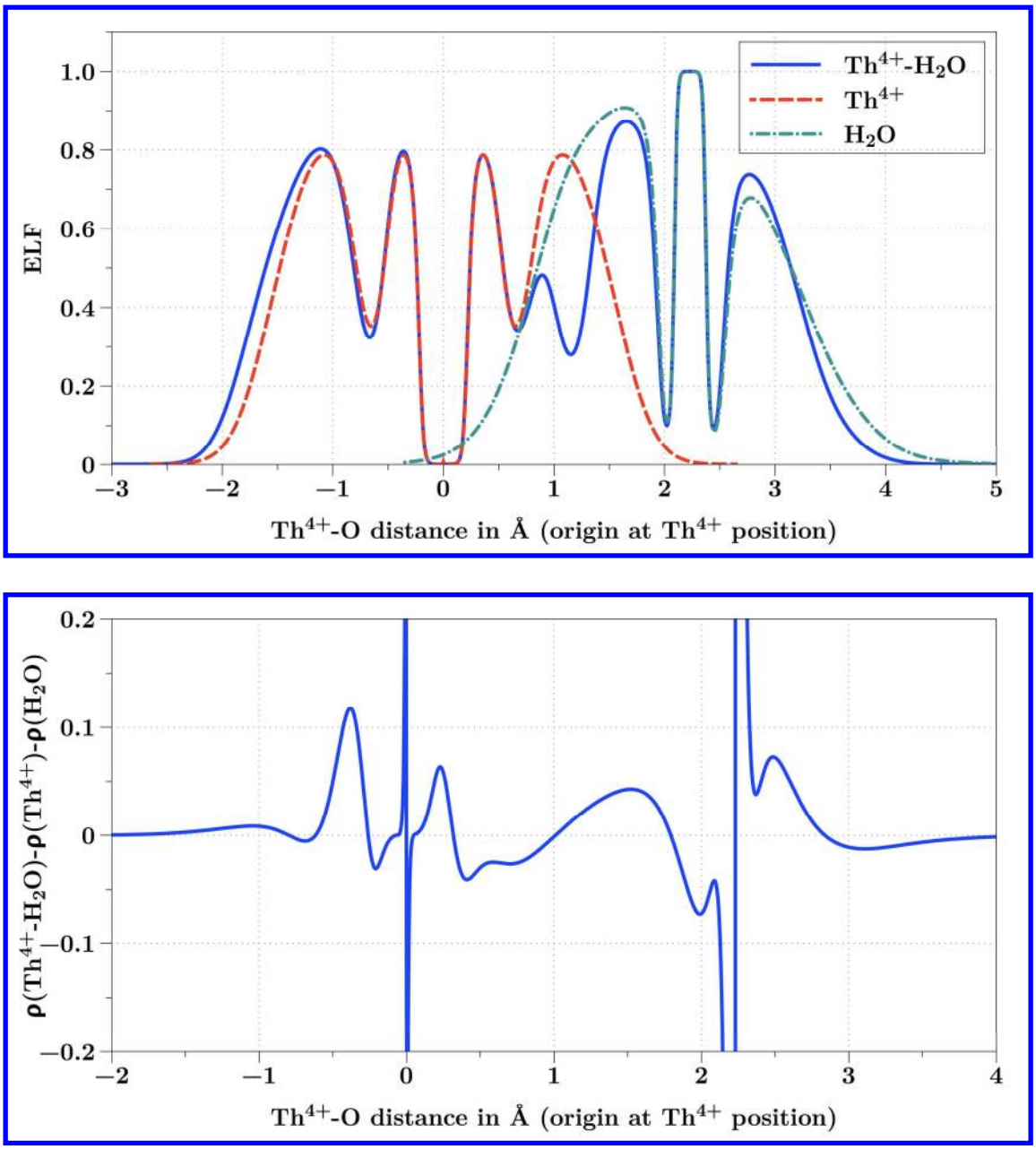


**Figure 2:** Values of the ELF function along the $C_2$ axis of the complex and of the fragments (top). Difference in electronic density between the complex and the fragments (bottom). Calculation Done with SET 2.

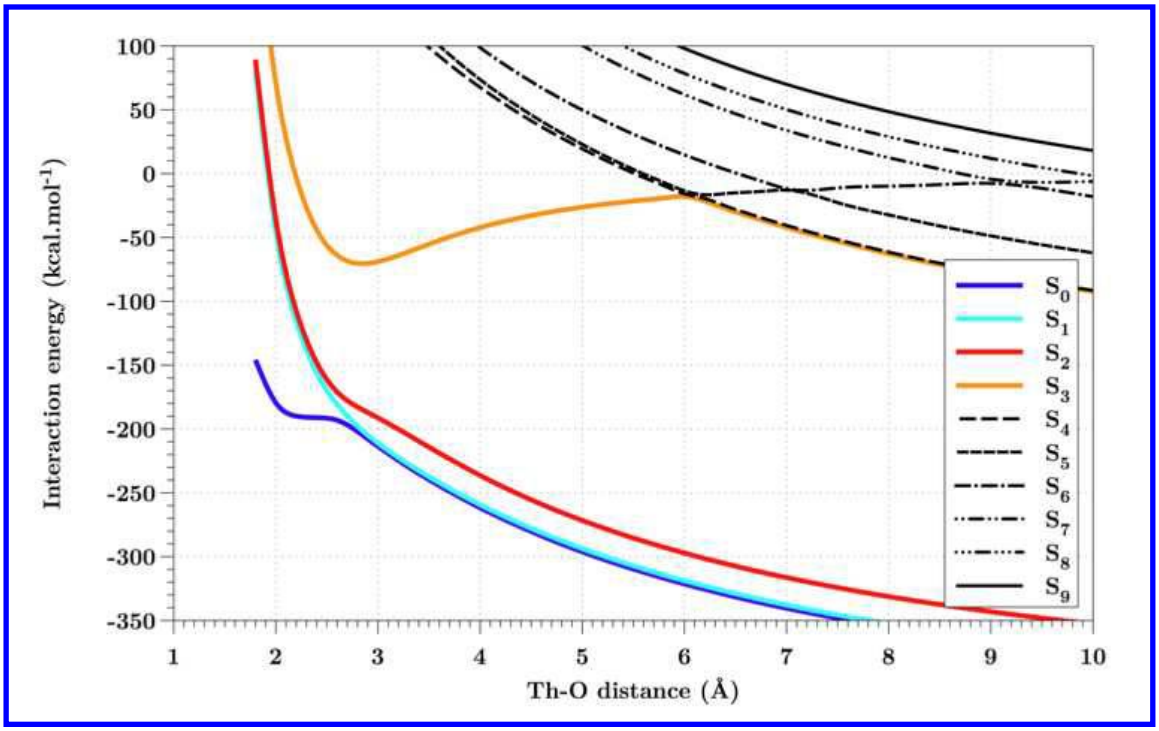


**Figure 3:** MCSCF adiabatic dissociation curve for $[Th(H_2O)]^{4+}$. Results obtained with SET 2.

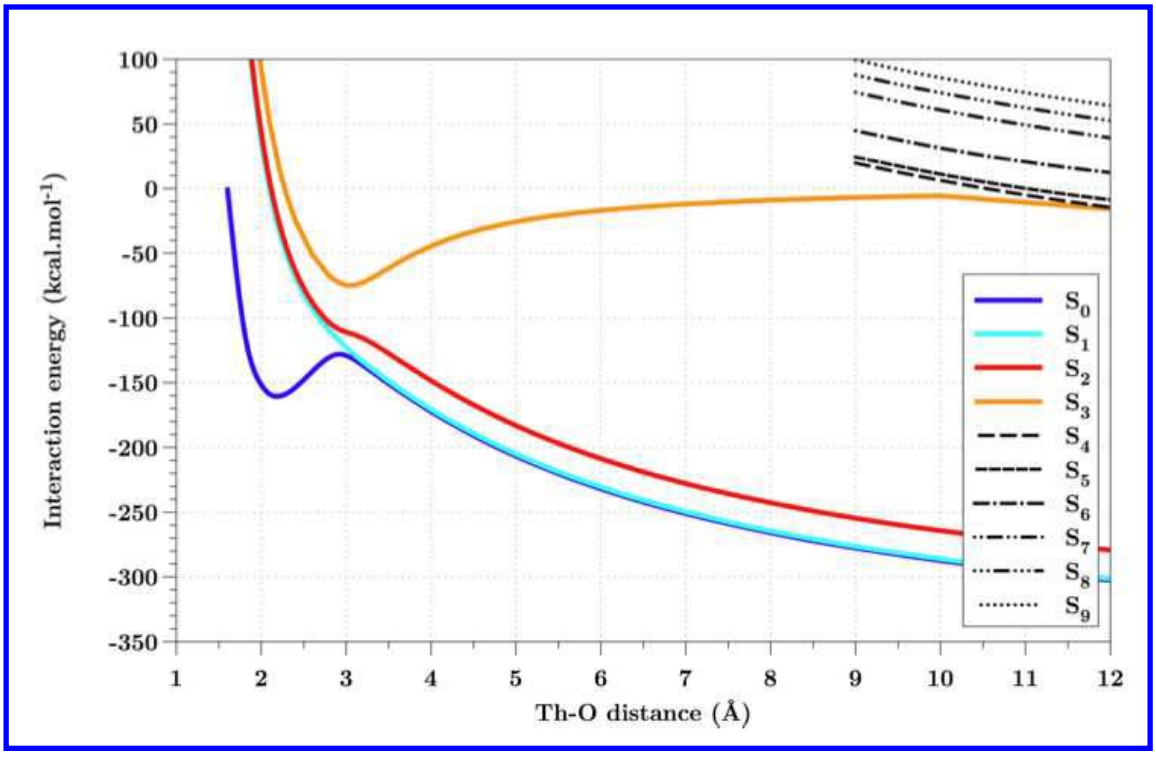


**Figure 4:** MRCI adiabatic dissociation curve for $[Th(H_2O)]^{4+}$ from a set of MCSCF configurations. Results obtained with SET 2.

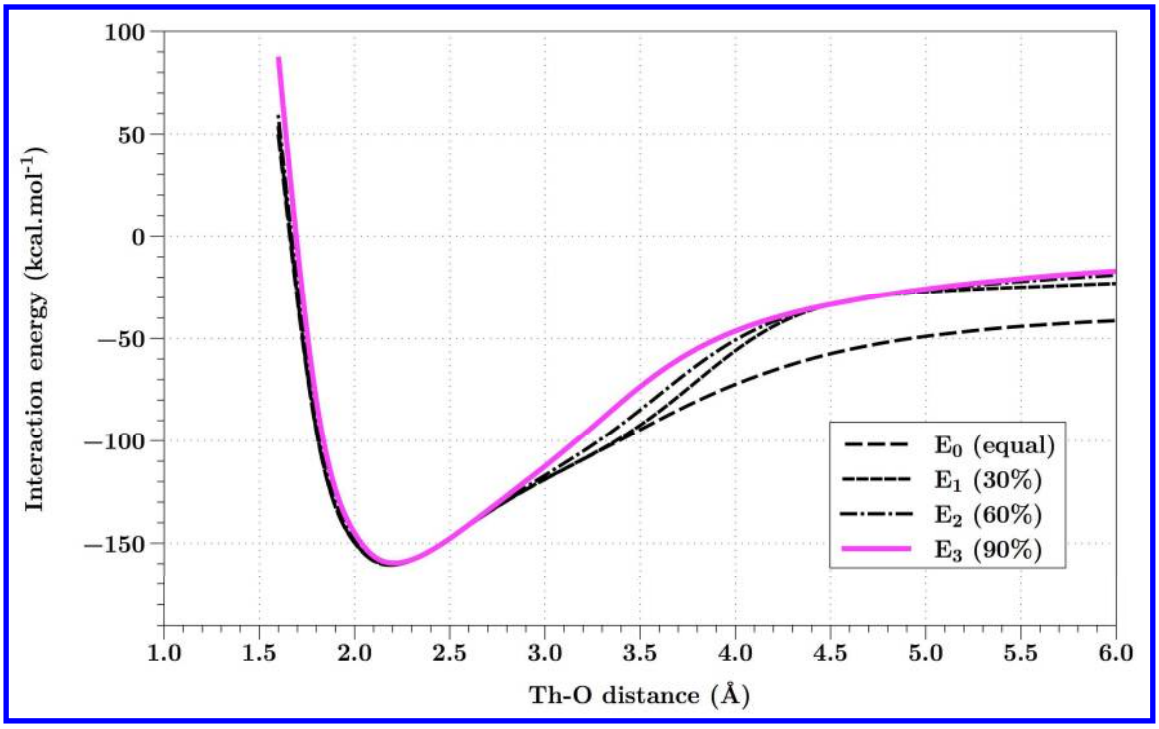


**Figure 5:** MRCI diabatic dissociation curve for $[Th(H_2O)]^{4+}$ using equilibrium geometry as reference and varying the weight of the different states. Results obtained with SET 2.

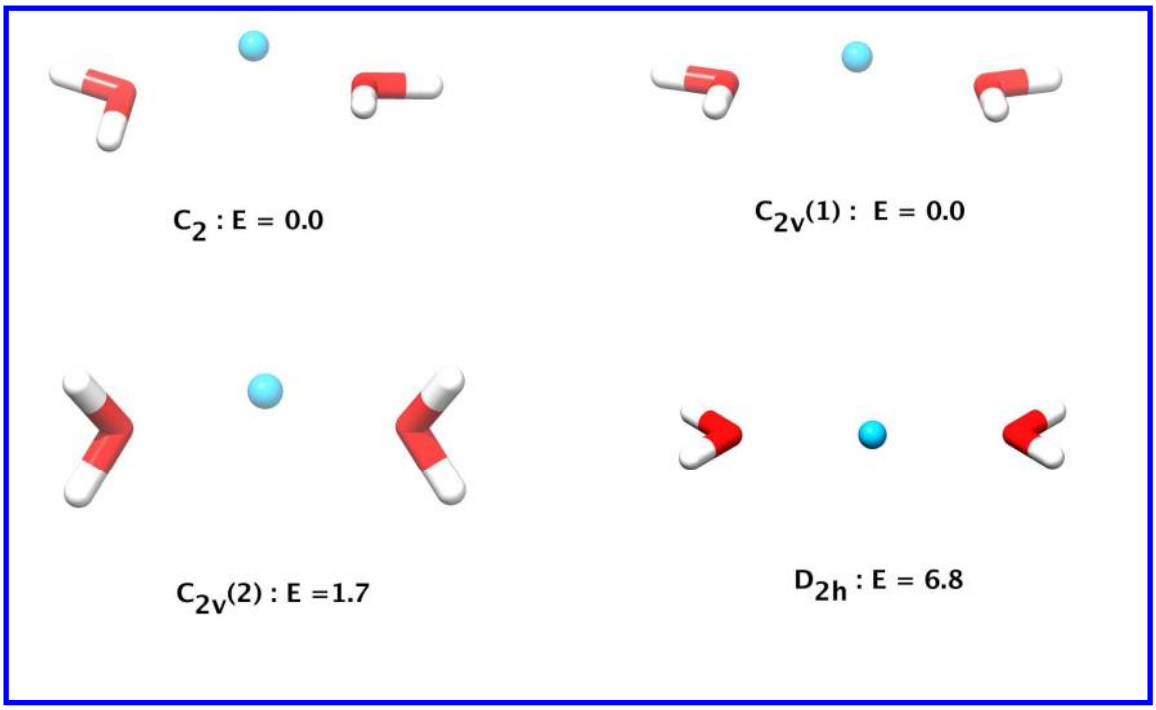


**Figure 6:** Structures of the $[Th(H_2O)_2]^{4+}$ complex and relative energies ($kcal.mol^{-1}$) (see Table 5) at MP2 level. Results obtained with SET 2.

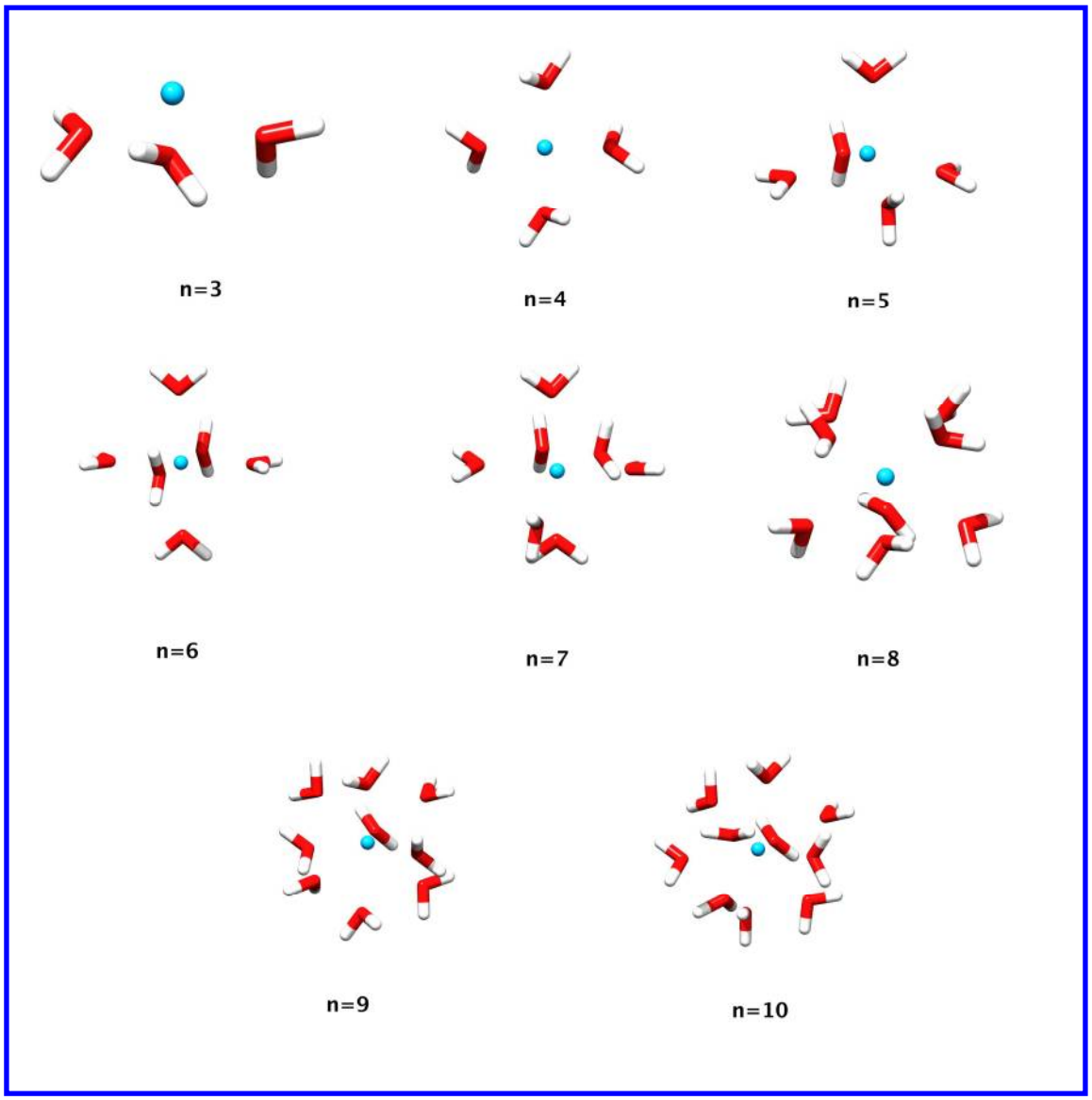


**Figure 7:** Structures of the most stable conformation of the $[Th(H_2O)_n]^{4+}$ complexes (n = 3 to 10). Results obtained with SET 3.

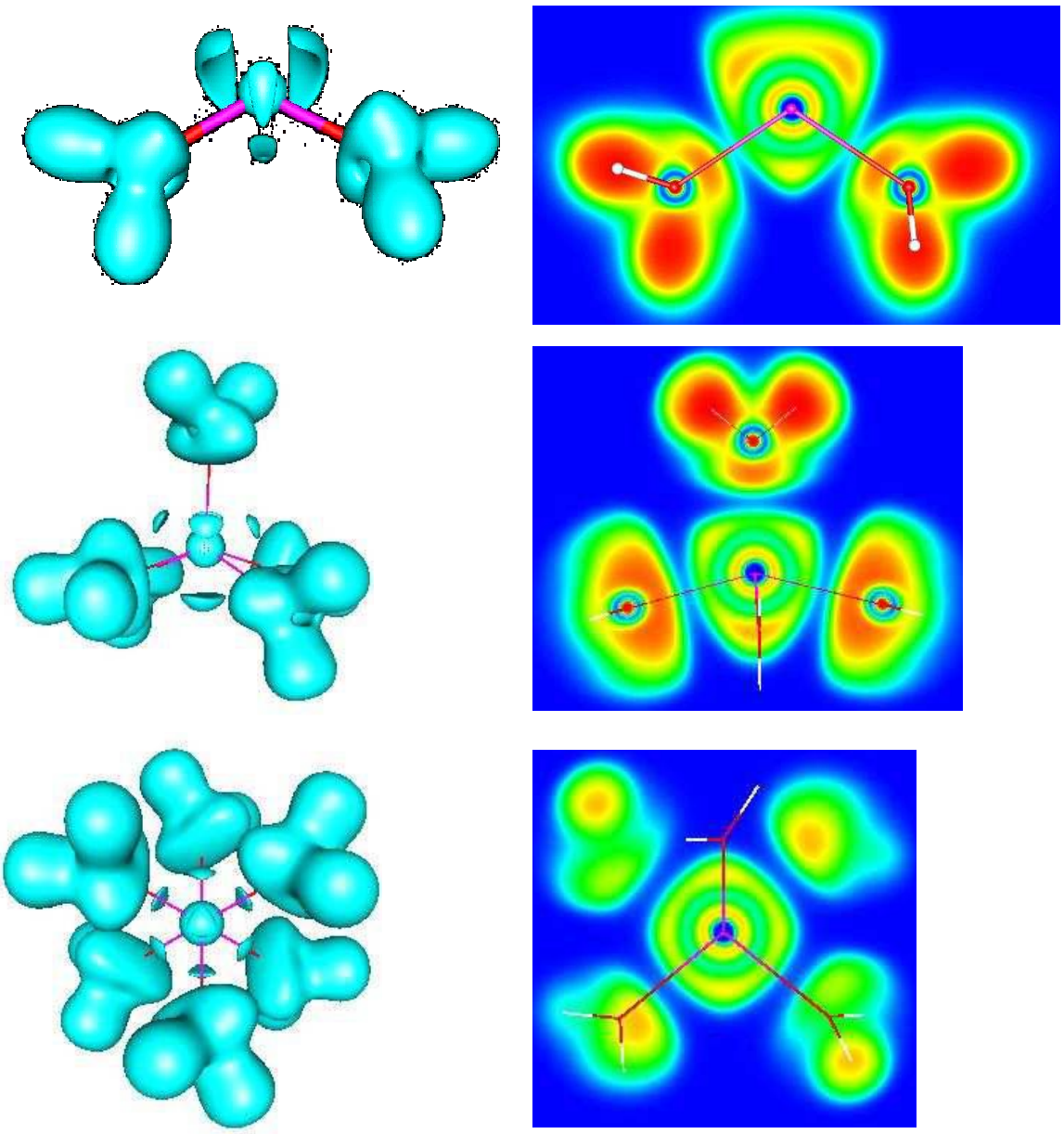

**Figure 8:** 3D ELF representation (left, η = 0.77) and cutplane representation (right) of the $[Th(H_2O)_2]^{4+}$ complex in $C_2$ symmetry (1st row), the $[Th(H_2O)_5]^{4+}$ (2nd row) and $[Th(H_2O)_6]^{4+}$ (3rd row) complexes. Results obtained with SET 3.

| Software | Level | Th-O | ΔE |
|---|---|---|---|
| DIRAC | NR-RHF | 2.163 | –159.4 |
| | SF-DHF | 2.217 | –147.1 |
| | DHF | 2.216 | –148.5 |
| MOLPRO | RHF | 2.216 | -147.8 |
| | MP2 | 2.189 | -161.5 |
| | CCSD | 2.197 | -158.8 |
| | CCSD(T) | 2.198 | -163.8 |
| | CI* | 2.194 | -156.7 |
| | PBE | 2.202 | -182.8 |
| | B3LYP | 2.199 | -171.7 |

**Table 1:** Th-O bond length (Å) and binding energies ΔE (kcal.mol$^{-1}$) of fully optimized $[Th(H_2O)]^{4+}$ complex at various level of approximation. * The CI binding energy is size consistency corrected using the Davidson method. Calculations with DIRAC are done with SET 1 and for MOLPRO with SET 2.

| N | Point Group | $E_{elec}$ | $E_{exrep}$ | $E_p(Th^{4+})$ | $E_p(OH_2)$ | $E_{ct}(Th^{4+})$ | $E_{ct}(OH_2)$ | $\delta E$ | $\Delta E$ |
|---|---|---|---|---|---|---|---|---|---|
| 1 | $C_{2v}$ | -105.8 | 74.2 | -2.5 | -60.7 | -0.1 | -45.7 | -3.5 | -144.2 |

**Table 2:** Energy decomposition analysis at the HF (in kcal.mol$^{-1}$) from $Th^{4+}$ and $H_2O$ fragments for the $[Th(H_2O)]^{4+}$ complex (see Computational details for the definition of the terms). Results obtained with SET 4.

| Method | n | 1 | 2 | 3 | 4 | 5 | 6 | 7 | 8 | 9 | 10 |
|---|---|---|---|---|---|---|---|---|---|---|---|
| HF | 7s | 0.00 | 0.02 | 0.04 | 0.06 | 0.09 | 0.12 | 0.14 | 0.16 | 0.17 | 0.18 |
| | 7p | 0.00 | 0.01 | 0.02 | 0.05 | 0.03 | 0.00 | 0.00 | 0.00 | 0.24 | 0.26 |
| | 5f | 0.04 | 0.06 | 0.08 | 0.10 | 0.15 | 0.21 | 0.25 | 0.19 | 0.16 | 0.02 |
| | 6d | 0.09 | 0.19 | 0.28 | 0.37 | 0.42 | 0.46 | 0.54 | 0.61 | 0.67 | 0.69 |
| MP2 | 7s | 0.00 | 0.01 | 0.04 | 0.05 | 0.08 | 0.12 | 0.13 | 0.15 | 0.17 | 0.18 |
| | 7p | 0.00 | 0.01 | 0.02 | 0.05 | 0.03 | 0.00 | 0.00 | 0.00 | 0.17 | 0.27 |
| | 5f | 0.04 | 0.07 | 0.09 | 0.11 | 0.16 | 0.23 | 0.28 | 0.21 | 0.24 | 0.02 |
| | 6d | 0.10 | 0.20 | 0.29 | 0.38 | 0.44 | 0.47 | 0.57 | 0.64 | 0.71 | 0.74 |
| B3LYP | 7s | 0.00 | 0.02 | 0.04 | 0.06 | 0.10 | 0.14 | 0.16 | 0.17 | 0.19 | 0.20 |
| | 7p | 0.00 | 0.00 | 0.02 | 0.04 | 0.05 | 0.00 | 0.11 | 0.07 | 0.25 | 0.27 |
| | 5f | 0.12 | 0.17 | 0.19 | 0.22 | 0.28 | 0.36 | 0.40 | 0.46 | 0.51 | 0.54 |
| | 6d | 0.14 | 0.29 | 0.42 | 0.55 | 0.63 | 0.67 | 0.76 | 0.84 | 0.90 | 0.93 |

**Table 3:** NPA population analysis of the Thorium ion accepting orbitals for $[Th(H_2O)_n]^{4+}$ (n=1 to 10) at HF, MP2 and B3LYP levels. Results obtained with SET 3.

| Method | Th-O distance | ΔE | ΔE + BSSE |
|---|---|---|---|
| HF | 2.233 | -146.4 | -146.2 |
| MP2 | 2.216 | -156.7 | -156.0 |
| CCSD | 2.220 | -154.8 | -154.3 |
| CCSD(T) | 2.222 | -156.7 | -156.0 |
| CI* | 2.216 | -152.7 | -152.1 |
| PBE | 2.236 | -176.3 | -176.1 |
| B3LYP | 2.227 | -166.5 | -166.3 |

**Table 4:** Th-O bond length (Å) and binding energies ΔE (kcal.mol$^{-1}$) of $[Th(H_2O)]^{4+}$ with frozen water molecule. * The CI binding energy is size consistency corrected using the Davidson method. Results obtained with SET 2.

| | Method | $C_2$ | $C_{2v}(1)$ | $C_{2v}(2)$ | $D_{2h}$ |
|---|---|---|---|---|---|
| Th-O | RHF | 2.286 | 2.285 | 2.290 | 2.316 |
| | MP2 | 2.263 | 2.263 | 2.268 | 2.293 |
| | PBE | 2.259 | 2.259 | 2.264 | 2.273 |
| | B3LYP | 2.259 | 2.259 | 2.264 | 2.278 |
| O-Th-O | RHF | 112.5 | 113.2 | 108.3 | 180.0 |
| | MP2 | 110.7 | 112.0 | 106.7 | 180.0 |
| | PBE | 117.8 | 118.1 | 115.4 | 180.0 |
| | B3LYP | 115.2 | 115.2 | 111.9 | 180.0 |
| O-Th-O-H | RHF | -14.6 | 0.0 | 90.0 | NC |
| | MP2 | -17.0 | 0.0 | 90.0 | NC |
| | PBE | -17.4 | 0.0 | 90.0 | NC |
| | B3LYP | 0.0 | 0.0 | 90.0 | NC |
| ΔE | RHF | 0.0 | 0.0 | 1.1 | 6.1 |
| | MP2 | 0.0 | 0.0 | 1.7 | 6.8 |
| | PBE | 0.0 | 0.0 | 1.5 | 3.1 |
| | B3LYP | 0.0 | 0.0 | 1.6 | 4.3 |

**Table 5:** Geometric parameters and relative energies ΔE (kcal.mol$^{-1}$) of the $[Th(H_2O)_2]^{4+}$ complexes at various levels of theory and for different symmetry groups. The Th-water distances (Th-O) are reported in Å, the water-Th-water angles and the out-of-plane angles between one water molecule and the O-Th-O plane are given in degrees. Results obtained with SET 2.

| | | Th-O distance | | | | O-Th-O angle | | | |
|---|---|---|---|---|---|---|---|---|---|
| | Sym | HF | MP2 | B3LYP | PBE | HF | MP2 | B3LYP | PBE |
| 1 | $C_{2v}$ | 2.230 | 2.210 | 2.200 | 2.202 | | | | |
| 2 | $C_2$ | 2.286 | 2.263 | 2.259 | 2.259 | 112.7 | 110.8 | 115.2 | 117.8 |
| 3 | $C_3$ | 2.332 | 2.307 | 2.307 | 2.302 | 106.9 | 103.2 | 107.1 | 108.4 |
| 4 | $S_4$ | 2.375 | 2.351 | 2.351 | 2.344 | 109.9 | 109.8 | 109.7 | 109.3 |
| 5 | $C_{2v}$ | 2.401 / 2.427 | 2.376 / 2.400 | 2.376 / 2.402 | 2.370 / 2.394 | 85.1 / 109.8 | 85.1 / 105.6 | 87.6 / 95.7 | 87.6 / 95.7 |
| 6 | $T_h$ | 2.459 | 2.427 | 2.433 | 2.425 | 90.0 | 90.0 | 90.0 | 90.0 |
| 7 | $C_2$ | 2.479 / 2.502 | 2.446 / 2.467 | 2.455 / 2.478 | 2.448 / 2.472 | 72.9 / 120.2 | 72.9 / 120.0 | 72.2 / 120.6 | 72.1 / 121.3 |
| 8 | $S_8$ | 2.526 | 2.489 | 2.505 | 2.498 | 73.1 / 77.8 | 73.3 / 77.5 | 73.0 / 78.0 | 73.1 / 77.8 |
| 9 | $D_3$ | 2.560 / 2.569 | 2.521 / 2.530 | 2.539 / 2.548 | 2.532 / 2.540 | 69.7 / 73.6 | 69.9 / 73.2 | 69.8 / 73.6 | 69.8 / 73.3 |
| 10 | $C_s$ | 2.570 / 2.656 | 2.531 / 2.610 | 2.545 / 2.641 | 2.538 / 2.634 | 68.3 / 128.2 | 67.9 / 128.5 | 67.9 128.6 | 67.6 / 128.5 |

**Table 6:** Structural parameters of the $[Th(H_2O)_n]^{4+}$ complexes n = 1 to 10. Extreme values of Th-O bond in Å and of the O-Th-O angle of neighboring water molecules in degrees. Results obtained with SET 3.

| | ΔE | | | | ΔE + ZPE + BSSE | | | | ΔG | | | |
|---|---|---|---|---|---|---|---|---|---|---|---|---|
| N | RHF | MP2 | PBE | B3L | RHF | MP2 | PBE | B3L | RHF | MP2 | PBE | B3L |
| 1 | -146.6 | -161.1 | -183.9 | -172.7 | -144.0 | -156.1 | -181.8 | -170.5 | -139.9 | -154.9 | -177.9 | -166.5 |
| 2 | -269.5 | -293.6 | -325.0 | -308.6 | -263.4 | -282.5 | -319.3 | -303.0 | -253.1 | -277.6 | -309.3 | -293.2 |
| 3 | -376.1 | -407.4 | -440.9 | -422.0 | -366.0 | -389.8 | -431.1 | -412.3 | -348.6 | -379.9 | -413.1 | -393.8 |
| 4 | -470.2 | -507.0 | -539.4 | -519.2 | -456.3 | -483.0 | -525.7 | -505.8 | -431.8 | -468.5 | -502.2 | -481.1 |
| 5 | -547.1 | -589.4 | -618.9 | -597.8 | -528.5 | -558.0 | -600.3 | -579.7 | -496.0 | -538.1 | -568.1 | -546.7 |
| 6 | -617.4 | -664.6 | -690.2 | -668.6 | -594.8 | -627.1 | -667.0 | -646.1 | -554.2 | -602.6 | -627.0 | -605.0 |
| 7 | -673.9 | -726.6 | -744.7 | -722.9 | -645.8 | -679.3 | -715.8 | -694.8 | -595.8 | -648.8 | -666.8 | -644.7 |
| 8 | -725.4 | -783.6 | -794.8 | -772.7 | -692.0 | -727.4 | -760.5 | -739.3 | -632.6 | -690.7 | -702.7 | -680.1 |
| 9 | -765.6 | -829.1 | -833.8 | -811.3 | -727.1 | -765.4 | -794.7 | -773.0 | -659.9 | -723.1 | -729.2 | -705.9 |
| 10 | -792.2 | -860.9 | -860.6 | -837.0 | -749.3 | -788.3 | -817.2 | -794.6 | -674.6 | -743.2 | -744.4 | -721.5 |

**Table 7:** Complexation energies in kcal.mol$^{-1}$ for the successive $[Th(H_2O)_n]^{4+}$ complexes with n varying from 1 to 10. ΔE is the electronic potential energy (first block). In the second block, it is corrected by the zero point energy (ZPE) and the basis set superposition error (BSSE). The third block contains the values of the gas phase free energies computed through the harmonic approximation. Results obtained with SET 3.